ORIGINAL ARTICLE

Validation of laser scanning confocal microscopy as a diagnostic method for lymphedema using a rat model

Song Jin[1] · Changlian Zhang[2] · Min Gao[3] · Ting Wang[4] · Lanbo Li[5] · Guoren Yang[3] · Yang Ou[3] · YunJie Li[6] · Sheng Li[3]

Abstract

Most previous diagnostic methods for lymphedema are invasive. Laser scanning confocal microscopy (LSCM) combines laser and computer image processing technology, is capable of increasing the resolution of optical microscopy by 30–40%, and boasts a comparable resolution to that of histological examination. We constructed the rat tail lymphedema model to simulate secondary lymphedema and to validate the noninvasive technique of in vivo reflectance LSCM for the diagnosis of lymphedema. The rat tail lymphedema model was constructed by cutting and ligating the lymphatic vessels in the rat tail. Lymphedema in the postoperative rat tail was assessed by a comprehensive range of methods including the change of rat tail diameter, lymphocytic radionuclide imaging, LSCM, and immunohistochemistry using a specific lymphatic vessel marker, prospero homeobox protein 1 (PROX1). The noninvasive LSCM method along with other techniques validated the rat tail lymphedema model. LSCM was used to perform qualitative and quantitative evaluation of the state and extent of lymphedema in the rat tail model. Receiver operating characteristic (ROC) curve analysis, which provided an area under the curve (AUC) value of 0.861, supported the feasibility of using LSCM as a reliable diagnostic technique for lymphedema. The rat tail lymphedema model can be successfully constructed by cutting and ligating the lymphatic vessels in the rat tail. Although LSCM cannot replace the method of skin biopsy examination, it offers a painless and noninvasive alternative for diagnosing lymphedema. Thus, LSCM can potentially be adopted in clinical practice as a supporting method to be used in combination with other techniques.

Keywords Secondary lymphedema · Laser scanning confocal microscopy · Diagnostic · PROX1

Abbreviations

LSCM	Laser scanning confocal microscopy
PROX1	Prospero homeobox protein 1
H&E	Hematoxylin and eosin
ICG	Indocyanine green
ROC	Receiver operating characteristic
AUC	Area under the curve

Song Jin, Changlian Zhang, YunJie Li and Sheng Li contributed equally to this work.

Electronic supplementary material The online version of this article (https://doi.org/10.1007/s10103-020-03106-y) contains supplementary material, which is available to authorized users.

✉ YunJie Li
  sdjnslyj@126.com

✉ Sheng Li
  drlisheng@sohu.com

[1] Department of Vascular Surgery, Affiliated Hospital of Jining Medical University, Jining 272029, China

[2] Department of Blood Transfusion, Rongcheng People's Hospital, Rongcheng 264300, China

[3] Shandong Cancer Hospital and Institute, Shandong First Medical University and Shandong Academy of Medical Sciences, No. 440, Jiyan Road, Jinan 250117, China

[4] Department of Pathology, Affiliated Hospital of Jining Medical University, Jining 272029, China

[5] Animal Laboratory, Qilu Hospital of Shandong University, Jinan 250012, China

[6] Logistics Support Department, Jinan Central Hospital Affiliated to Shandong University, No. 105 Jiefang Road, Jinan 250013, China

Purpose

Lymphedema is a complex disease characterized by lymphatic insufficiency. The typical clinical manifestations of lymphedema include numbness, swelling of the skin and subcutaneous tissue, and having the sensation of heavy pressure. Tissue with edema is prone to infection and causes inflammation of the lymphatic vessels and the surrounding tissues. In addition, there may be local symptoms of redness, swelling, heat, and pain, accompanied by high fever, chills, and other systemic symptoms. Chronic or primary lymphedema can occur in the skin, and subcutaneous tissue fibrosis and the Stemmer's sign may be observed [1]. Secondary lymphedema can arise due to filariasis, surgery, radiotherapy, trauma, repeated infections, tumor invasion, and metastasis [1]. Of note, filariasis-induced lymphedema was reported in more than 15 million people in developing countries according to a 2014 World Health Organization report. In addition, the number of tumor patients undergoing radical surgery and/or radiotherapy every year was found to be correlated with the incidence of secondary lymphedema [2]. Lymphedema can occur in women with breast cancer after they have undergone axillary lymph node dissection (30% probability) or melanoma inguinal lymph node dissection (20% probability) [3, 4]. There are few effective treatment methods for lymphedema; thus, intensive research in this area is urgently needed.

Due to the lack of radical treatment methods, early lymphedema detection is critical for preventing and managing the severity and progression of this disease. Although pathological biopsy examination is the gold standard for the reliable diagnosis of lymphedema, it being an invasive method is a major disadvantage. Hence, in this study, we explored the feasibility of noninvasive laser scanning confocal microscopy (LSCM) as an alternative diagnostic method for lymphedema.

Animal models are typically used to investigate the pathophysiological mechanisms of disease and to predict therapeutic effects in humans. Various methods may need to be used when constructing different disease models, and the choice of the appropriate animal model for use depends on the objective of the research. The canine model, which was constructed in the 1930s [5] by performing lymphatic ligation and the intralymphatic injection of sclerosing agents to the hindlimb of the dog, was the first chronic lymphedema model. After establishing the canine lymphedema model, the investigators subsequently found that radical lymphadenectomy and preoperative or postoperative radiotherapy [2, 6] were essential for the construction of a stable lymphedema model. Other researchers used a different method, lymphatic-venous anastomosis, to construct a secondary lymphedema canine model. Among the different anastomosis techniques, end-to-end anastomosis has shown low patency rates with vessels mostly blocked several weeks after surgery, while the patency rate was as high as 80% at 6 months after end-to-side anastomosis

[7–9]. A rabbit ear lymphedema model was proposed in 1976 [1], which was later proven to be a safe and reliable model of lymphedema. Construction of this model involves the microsurgical separation of lymphatic vessels at the base of the rabbit's ear. Since microsurgical reconstruction cannot be easily performed to treat lymphedema or vascularized tissue metastases, this technique is not directly applicable to the clinical setting. Another disadvantage of the rabbit ear model includes cartilage necrosis after perichondrial resection. Although the canine model bears historical value [10], it has been replaced by rodent models due to animal ethical issues, complex lymphatic edema induction methods, long duration for edema formation, high animal maintenance costs, high mortality, and the need for microsurgical techniques. Rodent models have been better received than other animal models due to their ready availability, cost-effectiveness, and ease of inducing and achieving stable lymphedema [11, 12]. The combination of radiation therapy and surgical methods has been shown to promote stable lymphedema effectively in the hindlimbs of rats and mice [13, 14]. In addition, the rodent tail lymphedema model [15] has been successfully used to study lymphedema treatment by surgery and gene therapy as well as to understand the molecular aspects of lymphangiogenesis [10, 16, 17].

In this study, we constructed the rat tail lymphedema model to simulate secondary lymphedema and to validate the noninvasive technique of in vivo reflectance LSCM for the diagnosis of lymphedema. LSCM combines laser and computer image processing technology, is capable of increasing the resolution of optical microscopy by 30–40%, and boasts a comparable resolution to that of histological examination [18]. We used this technique to observe the three-dimensional structure of the stratum spinosum epidermis in the rat tail, which is the site of lymph circulation and substance exchange in the skin. Furthermore, we employed several other techniques to validate the rat tail lymphedema model and as supporting methods for the LSCM results.

Methods

Creation of experimental lymphatic vascular insufficiency in a rat tail model

Post-surgical lymphedema was empirically induced in the tails of male Wistar rats (weighing 220–250 g; Jinan Pengyue Experimental Animal Breeding Co., Ltd.). The Wistar rats were randomly divided into three groups ($n = 6$ each): normal group, lymphedema group, and sham-operated group. In the lymphedema group, the rats were anesthetized with sodium pentobarbital (50 mg/kg intraperitoneally). Next, 0.1 mL of 2% methylene blue solution was injected intradermally into the end of the rat tail, and the tail was massaged for 3–5 min. The rat was then fixed in the prone

position on the operating table, and the skin was disinfected with iodine before an annular incision was made at 15 mm from the end of the tail. The skin and subcutaneous tissue were removed until the dermis layer, and the superficial lymphatic network was cut. The muscles, tendons, bones, and major blood vessels below the dermis were left untouched. A surgical microscope (Olympus, Japan) was used to visualize the two deep lymphatic vessels stained with methylene blue on the caudal side, and the vessels were sutured with 6–0 silk thread and cut. The sutured vessels were approximately 5 mm from the annular incision. The edge of the suture was cauterized with an electric knife to induce hemostasis [19]. In the sham-operated group, only the skin incision was performed, and the lymphatic vessels were not sealed. No surgery was performed for the normal control group. These three groups of rats were anesthetized so tissue from their tails could be sampled for all experiments. This study was approved by the Animal Ethics Committee of Shandong Cancer Hospital and Institute, China. All methods were performed in accordance with the relevant guidelines and regulations.

Measurement of tail diameter

A caliper was used to measure the diameter of the tail at a position 20 mm from the proximal end of the rat. The diameter of the rat tail was measured before surgery and at different timepoints (1, 3, 5, 7, 9, 11, 14, 21, 28, 35, and 42 days) after surgery. Of note, lymphedema-induced changes in the rat tail diameter were statistically significant between 2 and 21 days after surgery, while minimal changes were observed for the other assessed timepoints. Thus, we decided on 42 days post-surgery as the endpoint of measurement [10, 16, 17]. To account for the inherent differences between individual rats, the rate of change in the tail diameter was used to assess the change in rat tail diameter. Rate of change of rat tail diameter = (postoperative rat tail diameter − preoperative rat tail
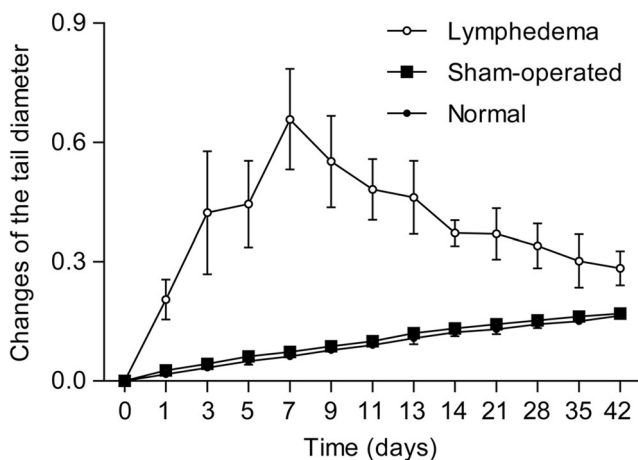
diameter)/preoperative rat tail diameter. Single-blind examination of the rat tail diameter was performed.

Lymphocytic radionuclide imaging

On day 7 post-surgery, radionuclide imaging was performed to assess the edema and the lymphatic drainage ability of the rat tail as well as to diagnose lymphedema. At room temperature, 0.2 mL of lymphoid imaging agent (Tc-99m ASC; Shihong Drug Development Center, Beijing, China) was injected intradermally to anesthetize the rats at 1 h before radionuclide imaging. Planar scanning (140 keV) was performed using a SPECT dual-probe instrument to record the lymphatic reflow image at 1 h after the injection to monitor rat tail lymph node development. Images acquired by the SPECT system were analyzed to compare the changes in lymphatic drainage function between groups. Single-blind examination was performed by a nuclear medicine professional.

LSCM

A laser scanning confocal microscope (Lucid, Inc., Rochester, NY, USA) was used to observe edema due to acanthosis of the skin of the rat tail on day 7 post-surgery. The gray value of the spine cell layer was measured by ImageJ software (ImageJ 1.x, National Institutes of Health, USA). The average value of three measurements was calculated, and the lymphedema-induced changes between the groups were compared. Subsequently, comparison between the edema results determined by LSCM and prospero homeobox protein 1 (PROX1) immunohistochemistry was performed, and receiver operating characteristic (ROC) curve analysis was performed using the EmpowerStats statistical software package.

H&E staining

Skin tissue located 20 mm from the end of the rat tail was sectioned on day 7 post-surgery and was fixed in 4% paraformaldehyde overnight. The 5-μm sections were then embedded with paraffin and stained with hematoxylin and eosin (H&E).

Immunohistochemistry

Immunohistochemistry was performed to analyze the expression of the transcription factor PROX1 in skin tissue sections. Paraffin sections of 5-μm thickness were deparaffinized in xylene, rehydrated using a serial ethanol gradient, pretreated with heat-induced antigen retrieval solution in a pressure cooker, and then inactivated with 3% endogenous peroxidase for 10 min. The sections were then incubated with rabbit polyclonal anti-PROX1 primary antibody (1:500 dilution; Abcam) for 1 h at room temperature, followed by incubation with

Fig. 1 Plots showing the changes in the rat tail diameter
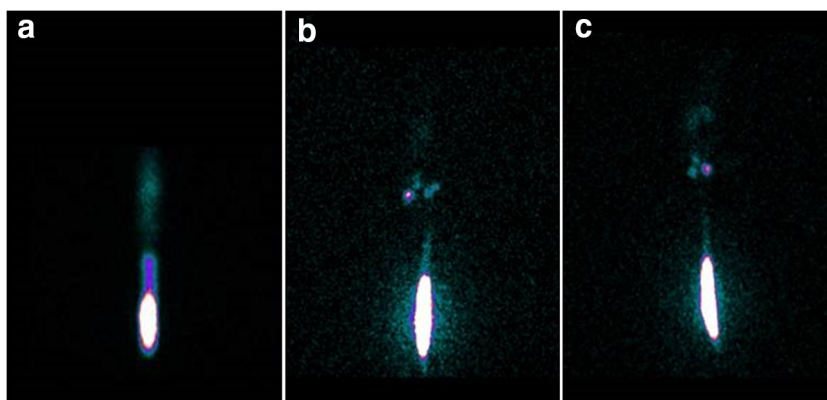
horseradish-peroxidase-conjugated anti-rabbit secondary antibody (Zhong Shan Jinqiao Biotechnology Co. Ltd., Beijing, China) for 30 min at room temperature, and finally detected with 3,3′-diaminobenzidine solution for 4 min. The tissue sections were counterstained with hematoxylin for 15 s and then dehydrated using a serial ethanol gradient before being covered with a coverslip.

Statistical analysis

Statistical analysis of the measured data was performed using the statistical software package EmpowerStats (http://www.empowerstats.com, X&Y Solutions, Boston, MA, USA). The analysis of variance test was performed to analyze the changes in the rat tail diameter, the intensity values of LSCM images, and the difference of the PROX1 immunohistochemical data between groups. Measurement data, assuming a normal distribution, were expressed as the mean ± standard deviation (SD), and count data were expressed as a percentage. The Kruskal–Wallis rank sum test was used to compare groups with a continuous variable. The Fisher's exact test was performed if the count variable has a theoretical value of < 10. A value of $P < 0.05$ was deemed statistically significant.

Results

Assessment of edema and rat tail diameter

In the lymphedema group, the tail started to swell on the first day after surgery. The swelling worsened and became most severe on the day 7 after surgery. Blisters were observed in cases of severe edema. On day 8 after surgery, edema in the tail gradually subsided. At 42 days after surgery, only mild swelling was observed. Although the surgical wound had healed, the skin of the tail was hard and fibrotic. Although the rat tail diameter for both the normal and sham-operated groups increased over the 42 days due to weight gain in both groups, this increase was not statistically significant ($P > 0.5$). On day 1 after surgery, the rat tail diameter in the lymphedema group was approximately 17–18% larger than that in the normal and sham-operated groups ($P < 0.0001$). Similarly, the rat tail diameter in the lymphedema group increased by approximately 58–59.5%, compared with the normal and sham-operated groups on day 7 after surgery (Fig. 1; Supplementary Tables 1 and 2; $P < 0.0001$).

Radionuclide imaging of rat tail lymphatic reflux

On day 7 after surgery, two rats in each group were subjected to rat tail lymphocyte imaging. In the lymphedema group,
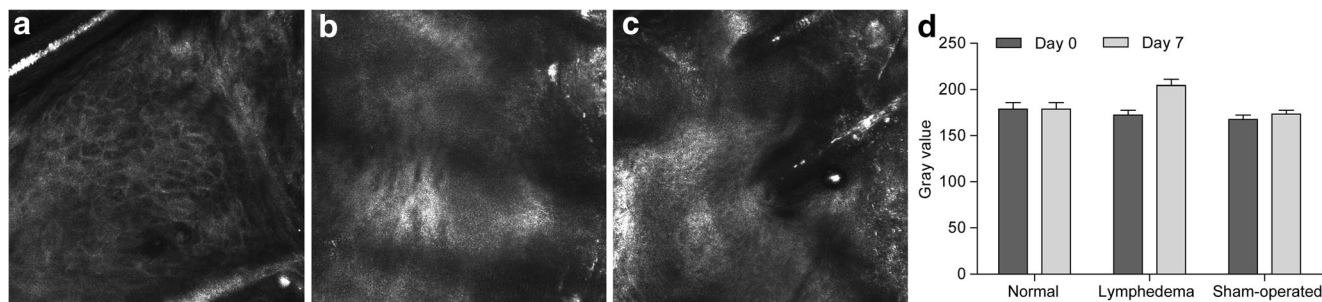

Fig. 3 Laser scanning confocal microscopy (LSCM) images of the skin of the rat tail for the **A** lymphedema, **B** normal, and **C** sham-operated groups on day 7 post-surgery at × 30 magnification. The spinous cell layer was uniformly distributed in the normal and sham-operated groups, but it was enlarged due to edema in the lymphedema group. **D** ImageJ analysis of the LSCM images of the skin of the rat tails of the lymphedema, normal, and sham-operated groups

Table 1 Analysis of the baseline gray value from laser scanning confocal microscopy of the skin of the rat tail

Time	Normal group	Lymphedema group	Sham-operated group
N	4	5	4
Day 0	178.87 ± 14.10	172.39 ± 11.49	167.62 ± 9.39
Day 7	181.42 ± 13.38	204.19 ± 15.19	173.35 ± 8.57

Mean ± SD

higher radionuclide tracer retention was observed in the subcutaneous areas of the surgical site and distal end, and the proximal lymphatic chain and lymph nodes were not developed (Fig. 2A); whereas in the normal group (Fig. 2B) and the sham-operated group (Fig. 2C), the lymphatic chain of the tail was well developed, and the pelvic bark had a defined round or oval shape. After the examination, one rat from the lymphedema group died, while two rats from the normal control and sham-operated groups died, respectively. The cause of death was due to individual differences among the rats and the low tolerance of certain rats to radionuclide exposure.

LSCM evaluation

Rats that still survived after completion of the radionuclide imaging experiment were taken forward for LSCM evaluation. The skin on the rat tail of the lymphedema ($n = 5$), sham-operated ($n = 4$), and normal (n = 4) groups was evaluated by LSCM before and on day 7 post-surgery. In the lymphedema group, edema resulted in translucency of the skin of the tail as well as the enlargement of the spinous cell layer, as evident from the increase in intensity of the transmitted light (Fig. 3A). However, in the normal (Fig. 3B) and the sham-operated (Fig. 3C) groups, the epidermis was clearly visible and a uniform distribution of cells in the spinous layer was observed. ImageJ analysis revealed no significant difference between the preoperative lymphedema group and the normal group ($P = 0.4315$). On day 7 post-surgery, the ImageJ-output transmission intensity value of the lymphedema group was notably higher on day 7 than on day 0

post-surgery, compared with that of the normal and sham-operated groups ($P < 0.05$; Figs. 3D; Tables 1 and 2).

Evaluation by H&E staining

On day 7 post-surgery, skin tissue located 20 mm from the end of the rat tail was stained by H&E. In the lymphedema group, marked acute inflammatory changes in the skin were observed: edema, hyperkeratosis, and spongiformity in the epidermis; uneven connection between the epidermis and the dermis; extension of the dermal papilla; and 2- to 3-fold tissue enlargement between the bone and the epidermis. In addition, significant changes in the cell structure, an increase in the number of fibroblasts and histiocytes, neutrophil infiltration, and granulated tissue were observed (Fig. 4A). A distinct boundary between the dermis and the epidermis as well as a normal cell architecture and morphology were observed in the normal and the sham-operated groups (Fig. 4B–C).

Immunohistochemical examination

Immunohistochemical examination was performed to determine the extent of lymphedema by semiquantitative assessment of the mean lymphatic count and the lymphatic vessel area. Monitoring of the changes in the lymphatic vessels of the rat tail skin sections was achieved by immunohistochemical labeling of PROX1, which is a specific marker of lymphatic vessels. The mean number of lymphatic vessels was determined by averaging the number of lymphatic vessels on each slide at ×400 magnification. The average numbers of lymphatic vessels in the lymphedema, normal, and sham-operated groups were 4.333 ± 0.816, 0.833 ± 0.408, and 1.000 ± 1.095, respectively (Fig. 5A–D; Table 3). There were 3.5 times more PROX1-positive lymphatic vessels observed in the lymphedema group compared with the normal and sham-operated groups ($P < 0.0001$).

The lymphatic area was measured by ImageJ image analysis software, and the mean value of three

Table 2 Univariate analysis of the laser scanning confocal microscopy data of the spinous cell layer of the skin of the rat tail

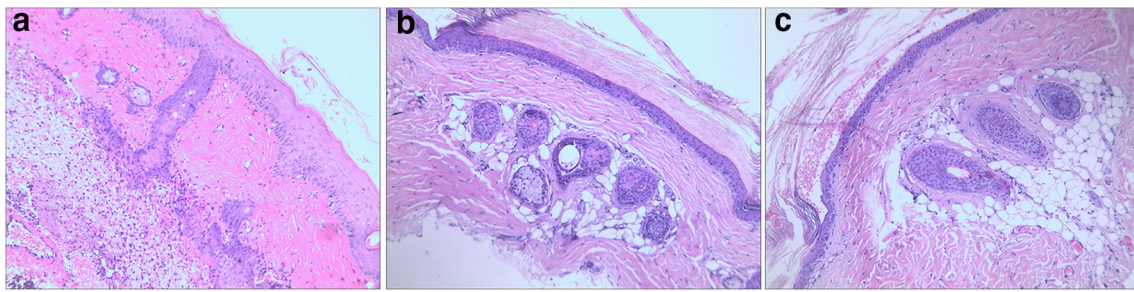| Group	Number	Before surgery		7 days after surgery	
		OR (95% CI)	P value	OR (95% CI)	P value
Normal group	4 (30.77%)	0		0	
Lymphedema group	5 (38.46%)	− 6.48 (− 21.98, 9.02)	0.4315	25.32 (7.98, 42.66)	0.0169
Sham group	4 (30.77%)	− 11.25 (− 27.59, 5.09)	0.2068	− 5.53 (− 23.80, 12.75)	0.5667

OR odds ratio, CI confidence interval

Fig. 4 H&E staining of the rat tail of the **A** lymphedema, **B** normal, and **C** sham-operated groups on day 7 post-surgery at ×100 magnification

independent lymphatic tube measurements was calculated. The mean areas of lymphatic vessels in the lymphedema, normal, and sham-operated groups were 0.037 ± 0.010 mm^2, 0.006 ± 0.004 mm^2, and 0.007 ± 0.006 mm^2, respectively (Fig. 5 A, B, C, and E; Table 3). The lymphatic area in the lymphedema group increased by 0.031 mm^2 compared with that of the normal control and sham-operated groups (Fig. 5E; Tables 3 and 4; $P < 0.0001$). The area under the curve (AUC) value from ROC curve analysis comparing the LSCM data and the PROX1 immunohistochemical data was 0.861 (Fig. 5F).

Discussion

The rodent model is by far the best animal model in terms of availability, simple and straightforward experimental manipulations, cost-effectiveness, and amenability to induction of stable lymphedema [11, 12]. Given the advantages of the rat tail model over the rat hindlimb model, such as a less complex anatomy, ease of surgical manipulation, and high reproducibility [15], we decided to establish the rat tail lymphedema model using the lymphatic ligation method.

Assessment of the rat tail lymphedema model was performed by a range of methods tested on three groups of rats:
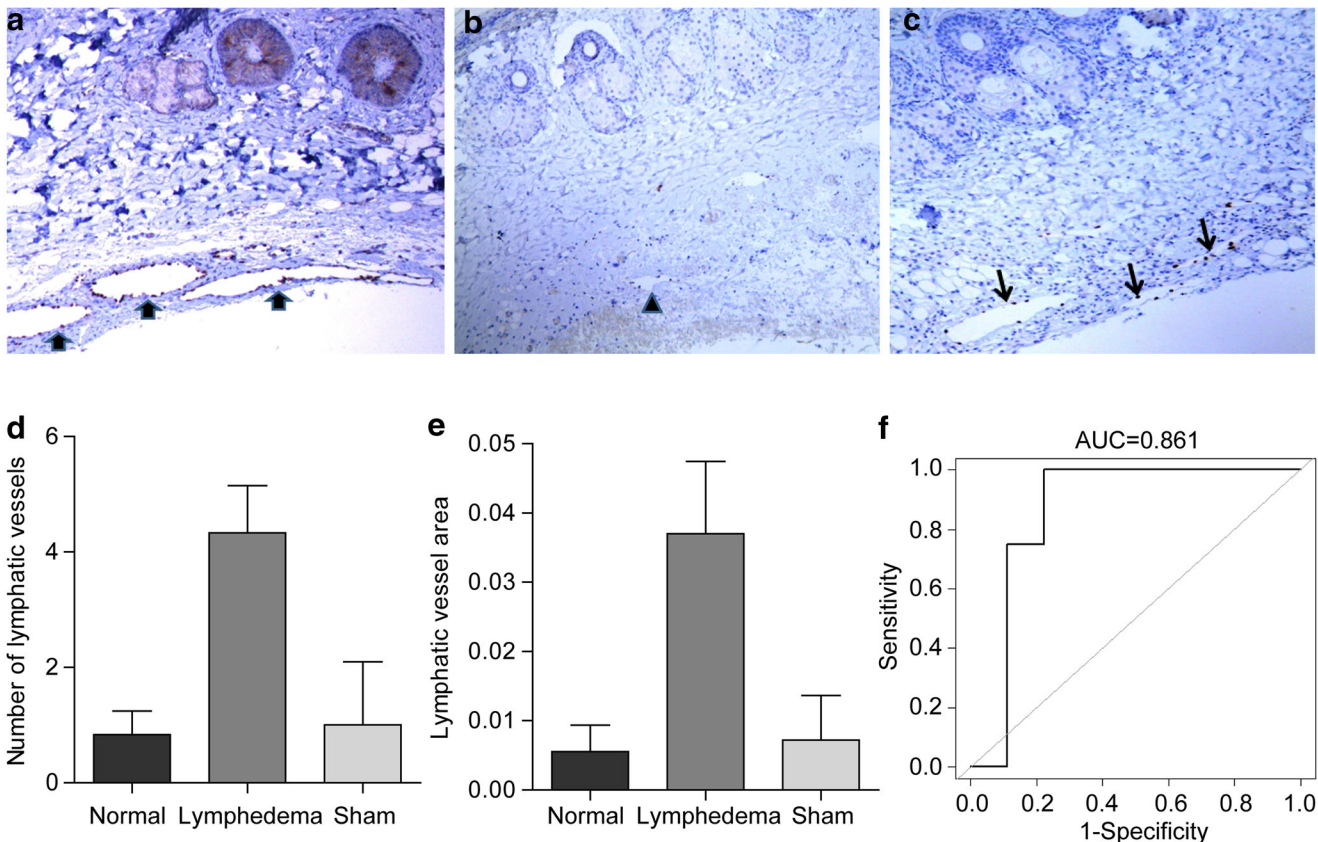

Fig. 5 Immunohistochemical images showing PROX1-positive lymphatic vessels in the skin sections of the **A** lymphedema group (thick arrow), **B** normal group (triangle), and **C** sham-operated groups (thin arrow) on day 7 post-surgery at ×400 magnification. Plots showing **D** the average number of PROX1-positive lymphatic vessels and **E** the mean lymphatic vessel area on day 7 post-surgery. **F** The ROC curve of the LSCM images

Table 3 Analysis of the baseline data of the mean lymphatic vessel count and lymphatic vessel area on day 7 post-surgery

Group	Normal group	Lymphedema group	Sham-operated group
N	6	6	6
Number of lymphatic vessels	0.833 ± 0.408	4.333 ± 0.816	1.000 ± 1.095
Area of lymphatic vessels (mm^2)	0.006 ± 0.004	0.037 ± 0.010	0.007 ± 0.006

Mean ± SD/N (%)

lymphedema, normal, and sham-operated groups. Postoperative edema, a higher rate of change in the diameter of the rat tail, and impaired lymphatic drainage were observed in the lymphedema group but not in the normal group. In addition, H&E-stained sections showed acute inflammation in the skin of the lymphedema group. Moreover, ImageJ analysis of the LSCM data revealed a higher light transmission in the lymphedema group compared with the normal group. Furthermore, as shown by immunohistochemistry, the mean lymphatic vessel count and lymphatic vessel area were significantly greater in the lymphedema group than in the normal and sham-operated groups. Taken together, our findings indicate the successful induction of lymphedema in the rat tail and the establishment of a rat tail lymphedema model. Additionally, the findings suggest that LSCM can be potentially applied in the clinical diagnosis of lymphedema.

It is difficult to diagnose lymphedema at an early stage as the blood vessels and lymphatic vessels are not easily distinguishable under light microscopy without prior injection of a paraffin-embedded tracer or an intravascular injection of latex [20]. Therefore, complex examination methods, such as lymphoscintigraphy, computed tomography, magnetic resonance lymphangiography, indocyanine green (ICG) near-infrared fluorescence imaging, and ICG lymphangiography, are often needed to confirm the presence of lymphatic drainage disorders [20–23]. The whole-fixation staining of specific markers, such as lymphatic vessel endothelial hyaluronan receptor 1, PROX1, and podoplanin, is necessary to enable the identification of lymphatic vessels and vascular structures in tissue sections [24]. In this study, we selected PROX1 as the specific marker to identify the lymphatic vessels in sections of the rat tail skin by immunohistochemistry. This transcription factor is highly expressed in the nucleus of lymphatic endothelial cells in a variety of tissues [25]. Since lymphedema is characterized by an increase in the number of lymphatic vessels, PROX1 was used to label the lymphatic vessels and to monitor changes in the lymphatic vessels. An increase in the number of PROX1-positive lymphatic vessels indicates the occurrence of lymphedema. Using this method, we were able to compare the occurrence of lymphangiogenesis in the lymphedema group to that in the normal and sham-operated groups.

Skin biopsy combined with immunohistochemistry can definitively diagnose lymphedema. But this is an invasive method that may increase the patient's mental stress, heighten the risk of incision infection, and delay healing [26]. Hence, we propose LCSM as an alternative diagnostic method for lymphedema. Specifically, we showed that LSCM can qualitatively and noninvasively assess the severity of the edema of the skin and subcutaneous tissue cells. In addition, semiquantitative analysis of the LSCM grayscale images could be determined with Image J image analysis software. To assess the diagnostic value of LSCM, ROC curve analysis was performed using the PROX1 immunohistochemical data as the reference for comparison. An AUC score of 1 indicates perfect coherence between the LSCM and immunohistochemical data, and a score of 0.5 indicates a failed test. The AUC value of 0.861 obtained in our study indicates that LSCM is a technique with certain diagnostic sensitivity and accuracy for detecting rat tail skin edema. However, LSCM cannot explain what causes edema of the skin and subcutaneous tissue. This method needs to be combined with other techniques to improve the specificity of diagnosis.

Although the current LSCM technology cannot replace skin biopsy, it can be used to diagnose lymphedema. Given its major advantage as a painless and noninvasive method for the diagnosis of skin edema at the cellular level, it could be applied in clinical practice in the near future.

Table 4 Univariate analysis of the mean lymphatic vessel count and the lymphatic vessel area on day 7 post-surgery

Group	Number	Number of lymphatic vessels		Area of lymphatic vessels (mm^2)	
		OR (95% CI)	P value	OR (95% CI)	P value
Normal group	6 (33.3%)	0		0	
Lymphedema group	6 (33.3%)	3.5 (2.6, 4.4)	<0.0001	0.031 (0.023, 0.040)	<0.00001
Sham group	6 (33.3%)	0.2 (−0.8, 1.1)	0.7	0.002 (−0.007, 0.010)	0.70279

OR (95% CI) P value

Conclusion

The rat tail lymphedema model can be successfully constructed by cutting and ligating the lymphatic vessels in the rat tail. Although LSCM cannot replace the method of skin biopsy examination, it offers a painless and noninvasive alternative for diagnosing lymphedema. Thus, LSCM can potentially be adopted in clinical practice as a supporting method to be used in combination with other techniques.

Code availability Not applicable.

Authors' contributions S.L. and Y.L. designed the experiments; S.J., C.Z., and Y.O. carried out the experiments; M.G. and G.Y. analyzed the data; T.W. and L.L. analyzed and interpreted the results; S.J. and C.Z. wrote the manuscript. All authors have read and approved the manuscript.

Data availability All data generated or analyzed during this study are included in this published article and its supplementary information files.

Compliance with ethical standards

Conflict of interest The authors declare that they have no competing interests.

Ethical approval This study was approved by the Animal Ethics Committee of Shandong Cancer Hospital and Institute, China.

Consent to participate Not applicable.

Consent for publication Not applicable.

References

1. Casley-Smith JR (1976) The medical treatment of lymphoedema. Experientia 32:825. https://doi.org/10.1007/bf02003705
2. Das SK, Franklin JD, O'Brien BM, Morrison WA (1981) A practical model of secondary lymphedema in dogs. Plast Reconstr Surg 68:422–428
3. McLaughlin SA, Wright MJ, Morris KT, Giron GL, Sampson MR, Brockway JP, Hurley KE, Riedel ER, Van Zee KJ (2008) Prevalence of lymphedema in women with breast cancer 5 years after sentinel lymph node biopsy or axillary dissection: objective measurements. J Clin Oncol 26:5213–5219. https://doi.org/10.1200/JCO.2008.16.3725
4. Stoberl C (1999) Indirect lymphography—possibilities and limits of roentgen diagnosis of the lymphatic system. Wien Med Wochenschr 149:92–94
5. Homans J, Drinker CK, Field M (1934) Elephantiasis and the clinical implications of its experimental reproduction in animals. Ann Surg 100:812–832. https://doi.org/10.1097/00000658-193410000-00022
6. Chen HC, Pribaz JJ, O'Brien BM, Knight KR, Morrison WA (1989) Creation of distal canine limb lymphedema. Plast Reconstr Surg 83:1022–1026. https://doi.org/10.1097/00006534-198906000-00016
7. Firica A, Ray A, Murat JE, Tompkins RK (1972) Alleviation of experimental lymphedema by lymphovenous anastomosis in dogs. Am Surg 38:409–412
8. Puckett CL, Jacobs GR, Hurvitz JS, Silver D (1980) Evaluation of lymphovenous anastomoses in obstructive lymphedema. Plast Reconstr Surg 66:116–120. https://doi.org/10.1097/00006534-198007000-00022
9. Al AF, Cordeiro AK, De Souza ECI (1988) A new technique of microlympho-venous anastomoses. Experimental study. J Cardiovasc Surg (Torino) 29:552–555
10. Hadamitzky C, Pabst R (2008) Acquired lymphedema: an urgent need for adequate animal models. Cancer Res 68:343–345. https://doi.org/10.1158/0008-5472.CAN-07-2454
11. Wang GY, Zhong SZ (1985) A model of experimental lymphedema in rats' limbs. Microsurgery 6:204–210. https://doi.org/10.1002/micr.1920060404
12. Kanter MA, Slavin SA, Kaplan W (1990) An experimental model for chronic lymphedema. Plast Reconstr Surg 85:573–580. https://doi.org/10.1097/00006534-199004000-00012
13. Lee-Donaldson L, Witte MH, Bernas M, Witte CL, Way D, Stea B (1999) Refinement of a rodent model of peripheral lymphedema. Lymphology 32:111–117
14. Oashi K, Furukawa H, Oyama A, Funayama E, Hayashi T, Saito A, Yamamoto Y (2012) A new model of acquired lymphedema in the mouse hind limb: a preliminary report. Ann Plast Surg 69:565–568. https://doi.org/10.1097/SAP.0b013e31821ee3dd
15. Slavin SA, Van den Abbeele AD, Losken A, Swartz MA, Jain RK (1999) Return of lymphatic function after flap transfer for acute lymphedema. Ann Surg 229:421–427. https://doi.org/10.1097/00000658-199903000-00017
16. Cheung L, Han J, Beilhack A, Joshi S, Wilburn P, Dua A et al (2006) An experimental model for the study of lymphedema and its response to therapeutic lymphangiogenesis. BioDrugs 20:363–370
17. Rutkowski JM, Moya M, Johannes J, Goldman J, Swartz MA (2006) Secondary lymphedema in the mouse tail: lymphatic hyperplasia, VEGF-C upregulation, and the protective role of MMP-9. Microvasc Res 72:161–171. https://doi.org/10.1016/j.mvr.2006.05.009
18. Ma J, Zhang X, Lv Y, Zhao C, Li Q, Yang X, Zhao J (2015) Clinical application of confocal laser scanning microscopy for atypical dermatoses. Cell Biochem Biophys 73:199–204. https://doi.org/10.1007/s12013-015-0625-5
19. Tabibiazar R, Cheung L, Han J, Swanson J, Beilhack A, An A, Dadras SS, Rockson N, Joshi S, Wagner R, Rockson SG (2006) Inflammatory manifestations of experimental lymphatic insufficiency. PLoS Med 3:e254. https://doi.org/10.1371/journal.pmed.0030254
20. Yan A, Avraham T, Zampell JC, Aschen SZ, Mehrara BJ (2011) Mechanisms of lymphatic regeneration after tissue transfer. PLoS One 6:e17201. https://doi.org/10.1371/journal.pone.0017201
21. Munn LL, Padera TP (2014) Imaging the lymphatic system. Microvasc Res 96:55–63. https://doi.org/10.1016/j.mvr.2014.06.006

22. Lu Q, Delproposto Z, Hu A, Tran C, Liu N, Li Y, Xu J, Bui D, Hu J (2012) MR lymphography of lymphatic vessels in lower extremity with gynecologic oncology-related lymphedema. PLoS One 7: e50319. https://doi.org/10.1371/journal.pone.0050319

23. Kayiran O, De La Cruz C, Tane K, Soran A (2017) Lymphedema: from diagnosis to treatment. Turk J Surg 33:51–57. https://doi.org/10.5152/turkjsurg.2017.3870

24. Kong LL, Yang NZ, Shi LH, Zhao GH, Zhou W, Ding Q, Wang MH, Zhang YS (2017) The optimum marker for the detection of lymphatic vessels. Mol Clin Oncol 7:515–520. https://doi.org/10.3892/mco.2017.1356

25. Choi I, Chung HK, Ramu S, Lee HN, Kim KE, Lee S et al (2011) Visualization of lymphatic vessels by Prox1-promoter directed GFP reporter in a bacterial artificial chromosome-based transgenic mouse. Blood 117:362–365

26. Garza RR, Skoracki R, Hock K, Povoski SP (2017) A comprehensive overview on the surgical management of secondary lymphedema of the upper and lower extremities related to prior oncologic therapies. BMC Cancer 17:468. https://doi.org/10.1186/s12885-017-3444-9